

1 **Bimetallic polyaniline/silver–palladium nanocomposite for rapid**
2 **and sustainable degradation of eosin yellow dye from**
3 **wastewater**

4 NOOR ZAMAN¹, FARAH NAZ TALPUR¹, ABDUL QADEER LAGHARI^{2*}, JAMEEL
5 BAIG¹, ARSHAD IQBAL³, SHOUKAT ALI NOONARI⁴, ZULFIQAR ALI BHATTI²,
6 AMANA BALOCH¹, IMRAN HASSAN AFARIDI¹ and MASROOR ABRO²

7 ¹*National center of Excellence in Analytical chemistry, University of Sindh, Jamshoro, Sindh,*
8 *Pakistan, ²Process Simulation and Modeling Research Group, Chemical Engineering*

9 *Department, Mehran University of Engineering and Technology Jamshoro, Sindh, Pakistan,*

10 *³Chemical Engineering Department, Dawood University of Engineering and Technology,*

11 *Karachi, Pakistan and ⁴Department of Mechanical Engineering, Isra University, Hyderabad,*
12 *Sindh, Pakistan*

13 (Received 2 July, revised 14 August, accepted 1 October 2025)

14 *Abstract:* Eosin yellow (EY), a synthetic xanthene dye, is recognized for its
15 high toxicity, posing serious threats to human health and aquatic environments.
16 Chronic exposure to EY can result in skin irritation, respiratory disorders, and
17 potential long-term organ damage due to its persistent and bioaccumulative
18 nature. In this study, a polyaniline-based silver–palladium nanocomposite
19 (PANI/Ag–Pd) was synthesized *via* the co-precipitation method and employed
20 as an efficient nanocatalyst for the degradation of EY dye. The structural, mor-
21 phological and elemental properties of the synthesized nanocomposite were
22 characterized using UV–Vis spectroscopy, Fourier-transform infrared spectro-
23 oscopy (FTIR), scanning electron microscopy (SEM) and energy-dispersive
24 X-ray spectroscopy (EDX). The UV–Vis and FTIR analyses confirmed the
25 formation of the PANI/Ag–Pd nanocomposite with a notable red shift, indi-
26 cating electronic interaction among the constituents. SEM images demonstrated
27 the successful incorporation of Ag and Pd nanoparticles into the PANI matrix,
28 while EDX confirmed the elemental composition. The nanocomposite exhi-
29 bited remarkable photocatalytic performance under microwave irradiation,
30 achieving up to 96.63 % degradation of EY dye. This study highlights the
31 potential of PANI/Ag–Pd nanocomposites as a promising nanocatalyst for
32 water purification. These findings contribute to the development of polymer-
33 stabilized nanomaterials as effective candidates for the remediation of dye-con-
34 taminated wastewater.

35 *Keywords:* wastewater treatment; nanocomposite; degradation; EY dye.

*Corresponding author. E-mail: abdul.qadeer@admin.muet.edu.pk
<https://doi.org/10.2298/JSC250702073Z>

36

INTRODUCTION

37 In recent decades, advanced materials such as nanomaterials, polymer-based
38 systems and hybrids have attracted increasing scientific interest due to their
39 exceptional chemical and physical properties.^{1–4} Dyes are classified into azoic,
40 reactive, vat, sulphur, acidic, basic, disperse and direct.⁵ Over 10,000 commercially
41 existing dyes and 1 Mt dyes are prepared annually, containing 50 % as a
42 textile dye.⁶ About 10 % of dyestuff is discarded after drying and processing.⁷ 2
43 % of the dye component entered the aqueous matter and caused pollution.⁸ Many
44 are toxic and discharged into wastewater untreated, often in high concentrations.⁹
45 Long-term usage of water-containing dyes causes severe health issues. Dyes are
46 carcinogenic and mutagenic. These dyes have been associated with carcinogenic
47 effects in the kidney, bladder and liver, and may also contribute to skin irritation
48 and respiratory complications.^{10,11} The cationic/anionic nature dyes leads to reduced
49 amount of oxygen in the water, which is fatal for humans and aquatic life.¹²
50 Several methods are being investigated for dyes removal from wastewater, like
51 microbial-electro-fenton (MEF) technology,¹³ catalytic degradation,¹⁴ adsorption,¹⁵
52 coagulation–flocculation,¹⁶ electrochemical treatment,¹⁷ reverse osmosis¹⁸ and ion exchange.¹⁹

54 Among various treatment methods, advanced oxidation processes (AOPs)
55 have shown promise.²⁰ Photocatalytic degradation using metals and metal oxides
56 like Ag, Pd, TiO₂, ZnO and WO₃ has been explored,²¹ often enhanced with
57 additives like NaBH₄ to boost dye decolorization efficiency under sunlight.²²

58 Polymers have recently emerged as promising alternatives to conventional
59 nanomaterials due to their adjustable surface functionalities, superior mechanical
60 strength, high surface area, uniform pore distribution and easy regeneration pro-
61 perties. Polymers such as polyaniline (PANI), polythiophene (PTh), polyethyl-
62 eneimine (PEI) and polypyrrole (PPy) have gained significant research interest
63 for developing metal–polymer nanocomposites. These hybrid materials have
64 broad applications in photocatalysis, sensing, adsorption, thermoelectric, electro-
65 magnetics and batteries, as well as electroluminescent and electromechanical sys-
66 tems. Among these, PANI is one of the most widely explored conductive poly-
67 mers, owing to its electron-rich structure, environmental stability, low cost and
68 ease of synthesis and processing.^{23,24} Its multifunctionality has enabled its use in
69 a broad range of technologies such as lithium-ion batteries,²⁵ flexible elec-
70 tronics,²⁶ anti-corrosion coatings,²⁷ wastewater treatment, dye removal²⁸ and
71 printed electronics.²⁹ The PANI/Ag–Pd system offers several advantages over
72 traditional catalysts. The conductive PANI matrix enhances electron transfer and
73 provides high surface area for dye adsorption, while Ag and Pd nanoparticles
74 create abundant active sites and exhibit strong catalytic synergy. This combi-
75 nation enables faster degradation rates, lower energy input and higher stability
76 compared to single-metal or conventional catalysts. Additionally, the nanocom-

77 composite is reusable, environmentally benign, and effective under mild conditions,
78 making it a sustainable alternative for wastewater treatment applications.

79 It is often used as a π -conjugated polymer base for integrating wide-bandgap
80 semiconductors such as metal oxides and sulfides. These composites demonstrate
81 enhanced photocatalytic, optical and photoelectric characteristic.³⁰ Additionally,
82 PANI acts as a proficient electron donor and hole transporter under UV–Vis light
83 exposure. When combined with high-bandgap metals like Ag, Fe, TiO₂ or ZnO,
84 PANI facilitates electron excitation under photon irradiation. These photoexcited
85 electrons transferred to the conduction band of the metal components, promoting
86 the generation of reactive species such as superoxide (O₂[•]) and hydroxyl radical
87 (•OH) through reactions with water and oxygen, which then drive the degrada-
88 tion of eosin yellow (EY) dye. In addition to experimental strategies, theoretical
89 modeling and statistical optimization are essential for developing sustainable
90 treatment processes. Statistical and predictive modeling approaches, such as res-
91 ponse surface methodology (RSM), enable systematic evaluation of multiple
92 operating variables, reduce experimental effort and predict interactions that are
93 often overlooked in conventional one-variable-at-a-time studies. By optimizing
94 key parameters, RSM ensures maximum degradation efficiency under practical
95 conditions, strengthening the reliability and scalability of nanocomposite-based
96 wastewater remediation.

97 In this work, *in-situ* synthesis of a PANI/Ag–Pd nanocomposite demon-
98 strating excellent catalytic behavior, was performed. EY degradation perform-
99 ance of PANI/Ag–Pd nanocomposite was investigated under different composite
100 dose, dye dose, pH and reaction time. Subsequently, RSM was performed with
101 the purpose of process optimization. PANI/Ag–Pd nanocomposite could be a pot-
102 ential candidate in dye removal process owing to its easy synthesis, low pro-
103 duction cost and high degradation efficiency.

104 EXPERIMENTAL

105 *Chemicals and reagents*

106 All the laboratory grade chemicals, glassware and other items were bought from Sigma
107 Aldrich. Aniline (99.95 %) was used as precursor to synthesize for polyaniline polymer. Hyd-
108 razine (98 %) was used as strong reducing agent as facilitator for synthesis of silver–pallad-
109 ium nanoparticles. Silver nitrate (99.8 %) and palladium(II) chloride, (99.999 %) were used
110 for synthesis for silver–palladium nanoparticles. Ammonium persulfate (98 %) was used as
111 strong oxidizing agent as facilitator for synthesis of PANI/Ag–Pd nanocomposite. Sulfuric
112 acid (98 %) was added as a proton source to form the conductive emeraldine salt of poly-
113 aniline, while protonated aniline exhibits a higher oxidation potential than neutral aniline, thus
114 delaying the onset of polymerization. Eosin yellow (EY) dye (99 %) was used as degradation
115 agent. Sodium borohydride (98 %) was used to donate hydrogen atoms (or electrons), break-
116 ing down the dye molecules into less harmful by products.

117 *Synthesis of PANI/Ag–Pd*

118 PANI was synthesized by dissolving 1.86 mL of aniline in 200 mL of 0.1 M H₂SO₄,
 119 followed by the dropwise addition of 10 mL of 5 M APS and stirring for 8 h at room tem-
 120 perature. The product was filtered, washed with de-ionized water and dried. For the PANI/
 121 /Ag–Pd nanocomposite, 1 mL of 0.02 M AgNO₃ was mixed with 2 mL of 0.062 M hydrazine
 122 and stirred at 60 °C for 5 min. Then, 50 mL of 0.035 M PdCl₂ was added and stirred for 45
 123 min. Finally, 10 mL of the Ag–Pd solution was mixed with 0.05 g PANI and 10 mL APS, fol-
 124 lowed by filtration, washing with de-ionized water and vacuum drying at 60 °C for 12 h.

125 *EY dye degradation*

126 The degradation of EY dye was evaluated by monitoring the decrease in its characteristic
 127 absorbance peak using a UV–Vis spectrophotometer (Jasco V-530 UV–Vis spectrophoto-
 128 meter) in the range of 350–800 nm. Pure dimethylformamide (DMF) was used as the blank
 129 solvent to eliminate background interference. Absorbance was converted into concentration
 130 using a calibration curve as suggested in a previous study.³¹ Degradation efficiency was cal-
 131 culated from the relative decrease in absorbance with time according to Eq. (1). It was
 132 assessed under varying experimental conditions, including pH 1–11, nanocomposite dose,
 133 0.5–1.5 mg/L, initial EY dye concentration, 3–12 mg/L, and reaction time, 5–15 s. The sel-
 134 ected pH range is closely reported in previously published data, to study its significance:^{32,33}

$$135 \quad \text{EY dye degradation} = 100 \frac{c_0 - c_e}{c_e} \quad (1)$$

136 where c_0 and c_e are initial and equilibrium EY dye concentrations (mg/L).

137 *Characterization*

138 The FTIR analysis of the PANI/Ag–Pd nanocomposite, mixed with KBr and pressed into
 139 pellets, was carried out using a Shimadzu 8400S (Japan) spectrometer. The measurements
 140 were taken within the wavenumber range from 4000 to 400 cm⁻¹, with a resolution of 4 cm⁻¹,
 141 to identify the functional groups present in the nanocomposite. Additionally, the surface mor-
 142 phology, particle size and elemental composition of the synthesized PANI/Ag–Pd nanocom-
 143 posite were analyzed using a scanning electron microscope (SEM) equipped with an energy
 144 dispersive X-ray (EDX) system.

145 *Experiments design*

146 RSM was employed to assess the individual and interactive effects of four variables, A
 147 (pH), B (composite dose), C (EY concentration) and D (reaction time) on degradation effi-
 148 ciency using a bimetallic polyaniline/Ag–Pd nanocomposite. A central composite design
 149 (CCD) was applied to construct a three-level matrix with factors coded as -1 (low) and +1
 150 (high). Variable levels are detailed in Table I.

151 TABLE I. Level of parameters for central composite design (CCD)

Variable	Symbol	Level	
		Low (-1)	High (1)
Dose of composite, mg/L	A	0.5	1.5
Dose of dye, mg/L	B	3	12
pH	C	1	11
Time, s	D	5	15

152 The response analysis was performed using Design Expert 13 through a regression-based
 153 approach. The main influences of the input variables are denoted as *A*, *B*, *C* and *D*, while their
 154 combined or interaction effects are represented by terms such as *AB*, *AC*, *AD*, *BC*, *BD* and
 155 *CD*, along with the quadratic components *A*² and *B*². The relationship between the variables
 156 and the response was modeled using a second-order polynomial equation:

$$157 \quad Y = a_0 + \sum_{i=1}^n a_i X_i + \sum_{i=1}^n a_{ii} X_i^2 + \sum_{j=i+1}^n a_{ij} X_i X_j \quad (2)$$

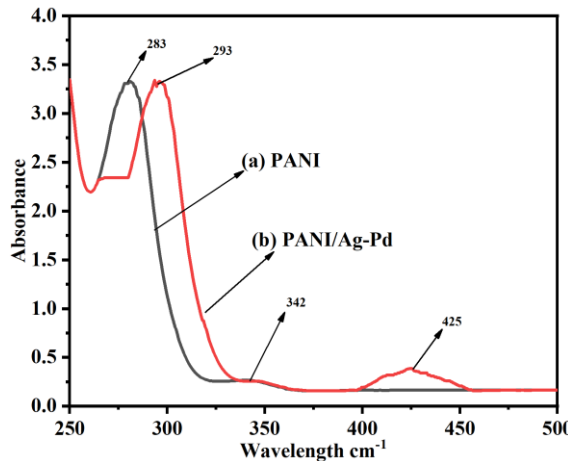
158 Where *Y* is predicted response, *X_i* are independent variables, *a₀* is constant (intercept), *a_i* are
 159 linear coefficients, *a_{ii}* are quadratic coefficients (squared terms) and *a_{ij}* are interaction
 160 coefficients (cross-product terms).

161 After each run, final concentration of EY dye was determined in order to find out the
 162 degradation in %.

163 RESULTS AND DISCUSSION

164 UV-Vis spectral analysis

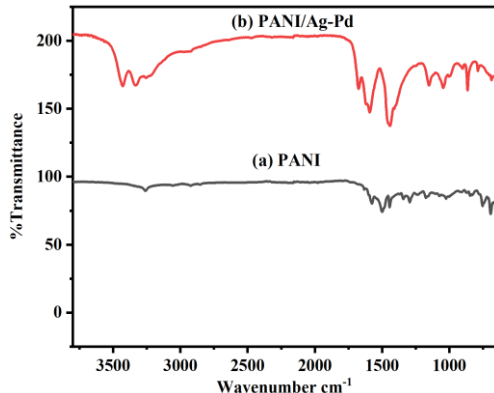
165 The UV-Vis spectra (Fig. 1) reveal key optical features of pure PANI and
 166 the PANI/Ag-Pd nanocomposite. Pure PANI shows peaks at 283 and 342 nm,
 167 indicating its doped state. In the composite, the $\pi-\pi^*$ peak shifts to 293 nm and a
 168 new band at ~425 nm appears, attributed to Ag/Pd surface plasmon resonance.
 169 These changes confirm nanoparticle incorporation and improved optical pro-
 170 perties, supporting its photocatalytic potential.



171
 172 Fig. 1. UV-Vis analysis of: a) PANI and b) PANI/Ag-Pd.

173 FTIR analysis

174 The FTIR spectrum illustrates the structural differences between pure poly-
 175 aniline (PANI) and the PANI/Ag-Pd nanocomposite, as shown in Fig. 2. The “a”
 176 spectrum corresponds to PANI, exhibiting characteristic peaks associated with its
 177 chemical structure. Notably, peaks in the ranges 1560–1580 and 1480–1500 cm⁻¹



178

179

Fig. 2. FTIR analysis of: a) PANI/Ag-Pd and b) PANI.

180 are associated with the C=C stretching vibrations of the quinoid and benzenoid
 181 structures in the polymer chain. The absorption band close to 1300 cm^{-1} is attri-
 182 buted to C–N stretching, while the signal near 1140 cm^{-1} corresponds to the in-
 183 plane bending of aromatic C–H bonds, which is commonly connected to the
 184 electrical conductivity characteristics of PANI. In contrast, the “b” spectrum rep-
 185 presents the PANI/Ag–Pd nanocomposite, which shows noticeable shifts in peak
 186 positions and variations in intensity, particularly in the 1500 – 1000 cm^{-1} region.
 187 These changes suggest strong interactions between the polyaniline matrix and the
 188 incorporated silver–palladium nanoparticles, likely through coordination with nit-
 189 urogen atoms in the PANI backbone. The appearance of a broader peak near 3400
 190 cm^{-1} may be attributed to N–H stretching or adsorbed water molecules. Overall,
 191 the spectral modifications confirm the successful incorporation of Ag–Pd nano-
 192 particles into the PANI structure, potentially enhancing the composite’s physico-
 193 chemical properties for applications such as dye removal or catalytic activity.

194 *Surface morphology characterization*

195 SEM was employed for the measurement of surface morphology of PANI/
 196 /Ag–Pd nanocomposite. The SEM images were taken at low and high resolution.
 197 These SEM images are shown in Fig. 3a and b at low and high resolutions. The

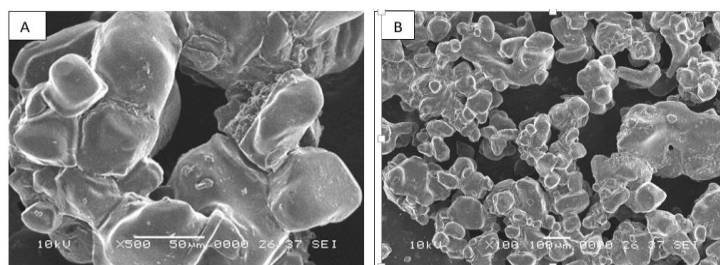
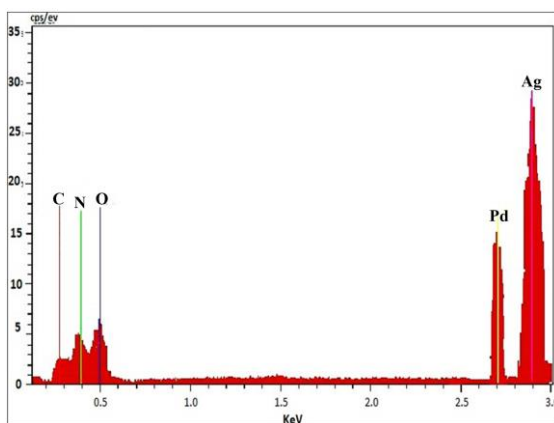


Fig. 3. The SEM images of: a) PANI and b) PANI/Ag–Pd.

198 SEM shows that structure of PANI/Ag–Pd nanocomposite is semi-cubical and
199 white dots are present due to the presence of PANI/Ag–Pd nanocomposite.
200 According to image, the silver and palladium particle were finely distributed
201 within the PANI matrix, although some accumulation and agglomeration were
202 observed in certain area.

203 *EDX analysis*

204 EDX analysis (Fig. 4) was employed to verify the elemental composition of
205 the PANI/Ag–Pd nanocomposite. The spectrum displays distinct peaks corres-
206 ponding to carbon, nitrogen and oxygen elements associated with the PANI mat-
207 rix. Additionally, the presence of characteristic peaks for silver and palladium
208 confirms the successful incorporation of metal nanoparticles into the composite
209 structure in K-shell with 1.99, 1.86 and 33.97 %, respectively. Silver and pal-
210 lidium were found in L-shell with 49.93 and 12.23 %.



211
212 Fig. 4. EDX analysis of PANI/Ag–Pd nanocomposite.

213 *EY dye degradation*

214 A comparative parametric analysis was conducted to evaluate the effective-
215 ness of various factors (pH, nanocomposite dose, initial dye concentration and
216 reaction time) influencing the degradation of the EY dye using a PANI/Ag–Pd.
217 The progressive degradation of the dye in the presence of PANI/Ag–Pd and
218 NaBH₄ was monitored *via* UV–Vis spectroscopy, as illustrated in Fig. 5. The
219 characteristic absorbance peak at approximately 336 nm exhibited a sharp decline
220 with increasing reaction time, indicating a rapid reduction in dye concentration.
221 At 5 s, the spectrum displayed the highest absorbance, corresponding to the ini-
222 tial dye concentration. Subsequent measurements at 10 s, showed a significant
223 decrease in peak intensity, while the peak was almost diminished at 15 s, indi-
224 cating almost total degradation. This continuous absorbance reduction witnesses

225 that UV–Vis spectroscopy effectively captured the real-time degradation behavior
 226 and highlights the efficiency of the PANI/Ag–Pd–NaBH₄ system, achieving most
 227 of dye removal within 15 s.

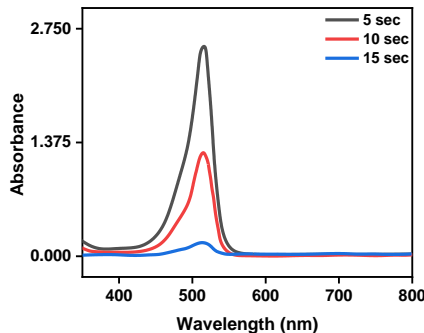


Fig. 5. UV–Vis spectra of dye degradation.

228 Experimental results revealed that a maximum degradation efficiency of
 229 96.63 % was achieved under optimal conditions: pH 5.8, nanocomposite dose,
 230 500 μ g/L, initial EY dye concentration, 900 μ g/L, and reaction time, 15 s; this
 231 was expected, as the integration of Ag–Pd enhances the availability of active
 232 binding sites, thereby improving the degradation efficiency.

233 *Response surface model results*

234 ANOVA and regression model results regression analysis was performed to
 235 predict EY dye degradation, considering factors *A*, *B*, *C* and *D*, along with their
 236 interactions (*AB*, *AC*, *AD*, *BC*, *BD*, *CD*), as summarized in Table II. The resulting
 237 equations show that positive coefficients indicate synergistic effects, while neg-

TABLE II. ANOVA for cubic model (response: EY dye degradation, %)

Source	Sum of squares	Df	Mean square	F-value	p-value	Significance
Model	16337.89	14	1166.99	102.39	< 0.0001	Significant
<i>A</i> -Dose of composite	85.97	1	85.97	7.54	0.0177	
<i>B</i> -Dose of EY	68.31	1	68.31	5.99	0.0307	
<i>C</i> -pH	2917.47	1	2917.47	255.96	< 0.0001	
<i>D</i> -Time	368.81	1	368.81	32.36	0.0001	
<i>AB</i>	0.0000	1	0.0000	0.0000	1.0000	
<i>AC</i>	123.19	1	123.19	10.81	0.0065	
<i>AD</i>	2.00	1	2.00	0.1756	0.6826	
<i>BC</i>	16.70	1	16.70	1.47	0.2494	
<i>BD</i>	7.428E-06	1	7.428E-06	6.517E-07	0.9994	
<i>CD</i>	361.48	1	361.48	31.71	0.0001	
<i>A</i> ²	127.14	1	127.14	11.15	0.0059	
<i>B</i> ²	13.58	1	13.58	1.19	0.2964	
<i>C</i> ²	10061.46	1	10061.46	882.74	< 0.0001	
<i>D</i> ²	204.33	1	204.33	17.93	0.0012	

238 ative ones suggest antagonistic impacts. These effects were analyzed to evaluate
 239 their influence on the model.

240 *ANOVA for cubic model*

241 The model demonstrates strong statistical significance, as indicated by a high
 242 *F*-value of 102.39 and a minimal probability (0.01 %), that this outcome is due to
 243 random variation. Variables *A*, *B*, *C* and *D*, as well as the interactions *AC*, *CD*,
 244 and the quadratic terms *A*², *C*² and *D*², significantly affect the response (*p* <
 245 < 0.0500). In contrast, terms with *p*-values above 0.1000 are considered statistically
 246 insignificant. Removing these non-significant terms while maintaining
 247 model hierarchy can improve model performance. Additionally, the lack of fit
 248 test produced an *F*-value of 1.15 with a 41.59 % probability, suggesting it is not
 249 statistically significant relative to pure error.

250 In the Table III the predicted *R*² of 0.9482 is in reasonable agreement with
 251 the adjusted *R*² of 0.9920; *i.e.*, the difference is less than 0.2. This demonstrates a
 252 reasonable correlation between experimental and predicted results of EY dye
 253 degradation.

254 TABLE III. Regression model equation for response against factors and their interaction

Regression model equation	<i>R</i> ²	Adjusted <i>R</i> ²
EY dye degradation (%) = 98.90 - 2.61 <i>A</i> - 2.50 <i>B</i> + 26.74 <i>C</i> - - 11.10 <i>D</i> + 0.0000 <i>AB</i> + 3.37 <i>AC</i> - 0.4868 <i>AD</i> + 1.25 <i>BC</i> + + 0.0010 <i>BD</i> + 11.13 <i>CD</i> - 7.16 <i>A</i> ² + 1.09 <i>B</i> ² - 29.33 <i>C</i> ² - 11.52 <i>D</i> ²	0.9917	0.9820

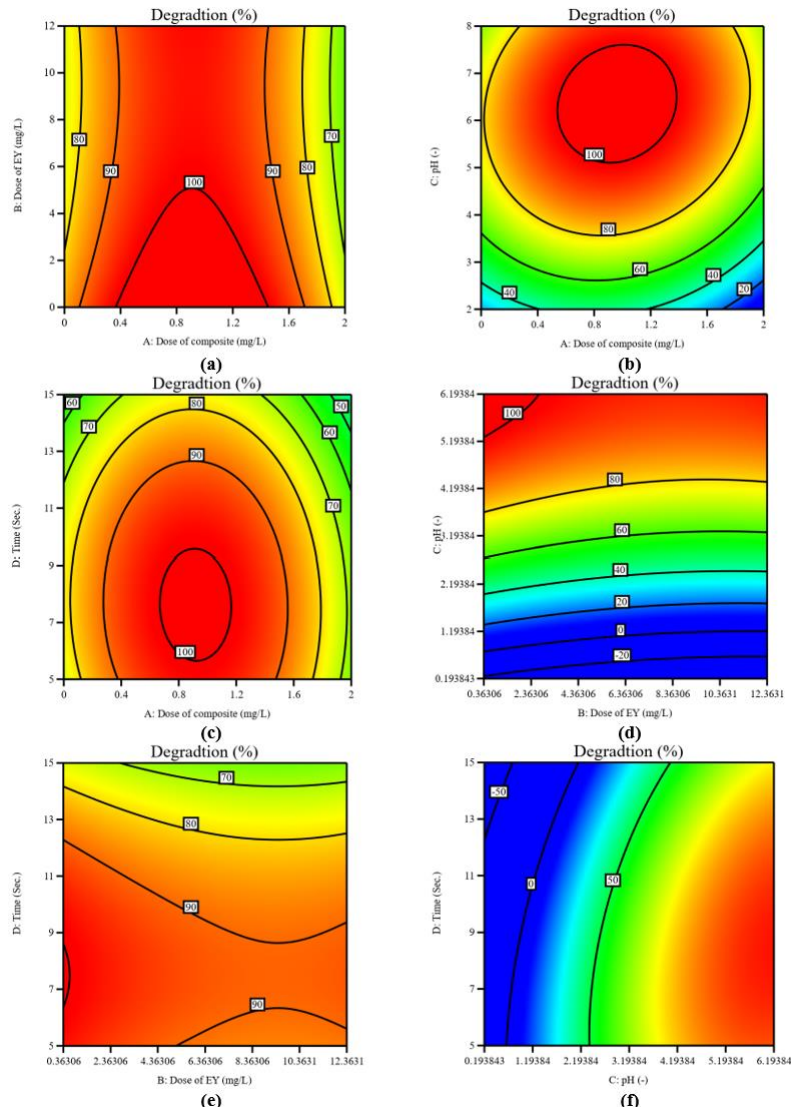
255 *Response contour plots*

256 Fig. 6 presents contour plots from RSM analysis, showing the interaction
 257 effects of key variables on EY dye degradation (%). Each plot illustrates the
 258 combined impact of two factors while keeping others constant. A color gradient
 259 from blue to red indicates increasing degradation efficiency. Results show that
 260 higher composite doses and lower pH levels significantly enhance degradation
 261 due to more active sites and increased •OH generation. In contrast, higher dye
 262 concentrations reduce efficiency.

263 *Performance evaluation of model*

264 Performance of model was evaluated by predicted vs. actual plot which
 265 visual representation of a model's accuracy, commonly used in regression
 266 analysis and machine learning to assess predictive performance.

267 In Fig. 7 the data points in this plot closely align with the diagonal line,
 268 indicating that the model has high accuracy and reliability in predicting EY dye
 269 degradation. The smooth color gradient suggests a well-fitted model without sig-
 270 nificant fluctuations and provides strong predictive performance for EY dye deg-
 271 radation.



272
273
274
275

Fig. 6. Contour plots of performance evaluation: a) dose of composite and dose of EY, b) dose of composite and pH, c) dose of composite and time, d) dose of EY and time, e) Dose of EY and time and f) pH and time.

276
277
278
279
280

Optimization of exponential parameters

Fig. 8 presents the optimized conditions for maximizing EY dye degradation using a composite, based on desirability function analysis from an RSM model. In solution 34 (out of 100), the optimal composite dose is 1.42706 mg/L and the EY concentration is 3.22423 mg/L, indicating that higher composite loading and

281 lower dye concentration enhance degradation. The optimal pH is 5.80, favoring
 282 dye–composite interaction, and the reaction time is short (6.01 min), showing
 283 rapid degradation. This setup achieves 99.69 % efficiency with a desirability
 284 value of 1.000, making it highly effective for wastewater treatment.

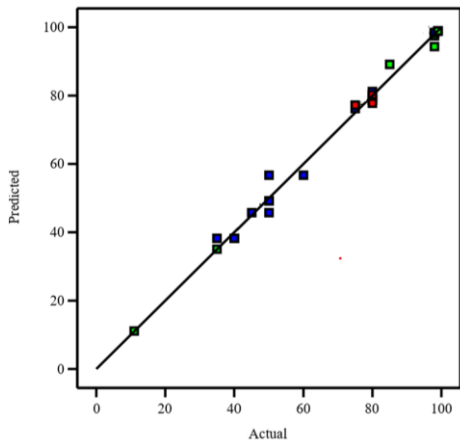
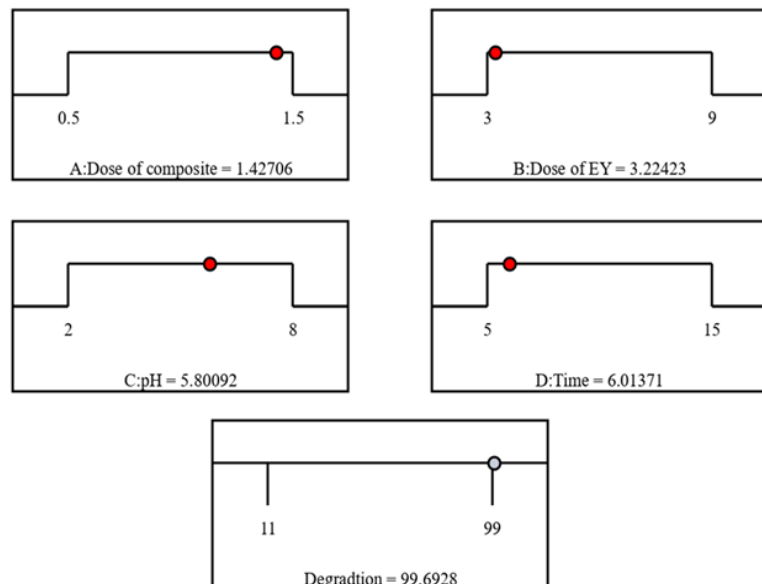


Fig. 7. Actual and predicted performance of model for EY dye degradation.



285
 286 Fig. 8. Optimization of experimental parameter using PANI/Ag–Pd.

287 *Comparison of EY dye degradation*

288 The results of dye degradation obtained in this study are benchmarked with
 289 those reported in previous literature. This comparative analysis (summarized in

Table IV) highlights the potential of presently used PANI/Ag–Pd nanocomposite towards achieving the remarkable dye removal (96.63 %) which can be attributed to the synergistic interaction between polyaniline and bimetallic Ag–Pd nanoparticles. While previous studies demonstrated the lower degradation efficiencies ranging from 92.30 to 99 %. However, these traditional composites require high material consumption and extended processing times. In contrast, the PANI/Ag–Pd system offers a rapid, energy-efficient and environmentally sustainable solution. Its low catalyst loading and ultrafast activity highlight its potential scalability for practical wastewater treatment. Future research should examine the stability and recyclability of this nanocomposite in real effluent conditions to confirm its applicability at industrial scale.

TABLE IV. Comparison of degradation of EY dye with earlier work reported

Composite	Dose of composite, mg/L	Time s	Dye dose mg/L	Degradation %	Ref.
Poly(pyrrole-co-aniline)-coated TiO ₂ /nanocellulose composite (P(Py-co-An)-TiO ₂ /NCC)	3500	5400	23.45	92.30	³⁴
New gold Salen complex doped carbon nanocomposite (Au–Salen/CC)	5000	3000	0.27	98.68	³⁵
TiO ₂ /tetra phenyl-porphyrin sulfonic acid nanocomposite (TiO ₂ /TPPS)	1100	3000	10.0	99.00	³⁶
PANI/Ag–Pd nanocomposite	1.42	360.6	3.0	96.63	This study

CONCLUSION

The study showed that PANI/Ag–Pd nanoparticles significantly enhance the degradation of eosin yellow (EY) dye. Characterization *via* UV–Vis, FTIR, SEM and EDX confirmed successful synthesis of the nanocomposite. Using central composite design with response surface methodology (RSM), optimal conditions 1.42706 mg/L composite dose, EY dose, 3.22423 mg/L, pH 5.80 and 6.01 min yielded 96.6 % degradation. These results highlight the nanocomposite's high catalytic efficiency and the effectiveness of RSM for process optimization in wastewater treatment. This work highlights the practical and environmental relevance of the PANI/Ag–Pd nanocomposite as a rapid, energy-efficient and sustainable material for wastewater remediation, offering a green alternative for treating dye-contaminated effluents. The ability to achieve such high degradation within seconds under mild conditions demonstrates its potential scalability for industrial applications. Future research should focus on long-term stability, recyclability, performance in real industrial wastewater and the extension of this approach to other toxic pollutants, thereby advancing the practical imple-

318 mention of nanocomposite-based catalytic systems in sustainable wastewater
319 management.

320 ИЗВОД

321 БИМЕТАЛНИ ПОЛИАНИЛИН/СРЕБРО-ПАЛАДИЈУМ НАНОКОМПОЗИТ ЗА БРЗУ И
322 ОДРЖИВУ ДЕГРАДАЦИЈУ ЕОЗИН ЖУТЕ БОЈЕ ИЗ ОТПАДНИХ ВОДА

323 NOOR ZAMAN¹, FARAH NAZ TALPUR¹, ABDUL QADEER LAGHARI², JAMEEL BAIG¹, ARSHAD IQBAL³, SHOUKAT
324 ALI NOONARI⁴, ZULFIQAR ALI BHATTI², AMANA BALOCH¹, IMRAN HASSAN AFARIDI¹ и MASROOR ABRO²

325 ¹National center of Excellence in Analytical chemistry, University of Sindh, Jamshoro, Sindh, Pakistan,

326 ²Process Simulation and Modeling Research Group, Chemical Engineering Department, Mehran University of
327 Engineering and Technology Jamshoro, Sindh, Pakistan, ³Chemical Engineering Department, Dawood
328 University of Engineering and Technology, Karachi, Pakistan и ⁴Department of Mechanical Engineering,
329 Isra University, Hyderabad, Sindh, Pakistan

330 Еозин жута (EY) синтетичка ксантонска боја је високо токсична, што представља
331 озбиљну претњу људском здрављу и воденим срединама. Хронично излагање EY може
332 довести до иритације коже, респираторних поремећаја и потенцијалног дугорочног
333 оштећења органа због његове упорне и биоакумулативне природе. У овој студији, нано-
334 композит сребра и паладијума на бази полианилина (PANI/Ag–Pd) синтетизован је
335 методом ко-таложења и коришћен као ефикасан нанокатализатор за разградњу EY боје.
336 Структурне, морфолошке и елементалне особине синтетизованог нанокомпозита су
337 окарактерисане коришћењем UV–Vis спектроскопије, Фурије-трансформисане
338 инфрацрвене спектроскопије (FTIR), скенирајуће електронске микроскопије (SEM) и
339 енергетски дисперзивне спектроскопије X-зрака (EDX). UV–Vis и FTIR анализе су
340 потврдиле формирање PANI/Ag–Pd нанокомпозита са значајним црвеним помаком, што
341 указује на електронску интеракцију између састојака. SEM слике су показале успешну
342 уградњу Ag и Pd наночестица у PANI матрицу, док је EDX потврдио је елементални
343 састав. Нанокомпозит је показао изванредне фотокатализичке перформансе под микро-
344 таласним зрачењем, постижући до 96,63 % деградације боје EY. Ова студија наглашава
345 потенцијал PANI/Ag–Pd нанокомпозита као обећавајућих нанокатализатора за пречи-
346 ђавање воде. Ови налази доприносе развоју наноматеријала стабилизованих полимером
347 као ефикасних кандидата за санацију отпадних вода контаминираних бојом.

348 (Примљено 2. јула, ревидирано 14. августа, прихваћено 1. октобра 2025)

349 REFERENCES

- 350 1. M. M. Shameem, S. Sasikanth, R. Annamalai, R. G. Raman, *Mater. Today: Proc.* **45**
351 (2021) 2536 (<https://doi.org/10.1016/j.matpr.2020.11.254>)
- 352 2. N. F. Alheety, A. H. Majeed, M. A. Alheety, *J. Phys.: Conf. Ser.* **1294** (2019) 052026
353 (<https://doi.org/10.1088/1742-6596/1294/5/052026>)
- 354 3. A. Kamal, M. Ashmawy, S. S. A. M. Algazzar, A. H. Elsheikh, *Proc. Inst. Mech. Eng., C*
355 **236** (2022) 4843 (<https://doi.org/10.1177/09544062211055662>)
- 356 4. L. A. Adnan, N. F. Alheety, A. H. Majeed, M. A. Alheety, H. Akbaş, *Mater. Today: Proc.* **42**
357 (2021) 2700 (<https://doi.org/10.1016/j.matpr.2020.12.707>)
- 358 5. S. El Harfi, A. El Harfi, *Appl. J. Environ. Eng. Sci.* **3** (2017) 311
359 (<https://doi.org/10.48422/IMIST.PRSM/ajees-v3i3.9681>)
- 360 6. P. Zarrintaj, M. K. Yazdi, H. Vahabi, P. N. Moghadam, M. R. Saeb, *Prog. Org. Coat.* **130**
361 (2019) 144 (<https://doi.org/10.1016/j.porgcoat.2019.01.053>)

362 7. M. Berradi, R. Hsisssou, M. Khudhair, M. Assouag, O. Cherkaoui, A. El Bachiri, A. El
363 Harfi, *Heliyon* **5** (2019) e02711 (<https://doi.org/10.1016/j.heliyon.2019.e02711>)

364 8. A. Kausar, M. Iqbal, A. Javed, K. Aftab, Z.-i.-H. Nazli, H. N. Bhatti, S. Nouren, *J. Mol.*
365 *Liq.* **256** (2018) 395 (<https://doi.org/10.1016/j.molliq.2018.02.034>)

366 9. E. Forgacs, T. Cserháti, G. Oros, *Environ. Int.* **30** (2004) 953
367 (<https://doi.org/10.1016/j.envint.2004.02.001>)

368 10. I. Ullah, A. Haider, N. Khalid, S. Ali, S. Ahmed, Y. Khan, N. Ahmed, M. Zubair,
369 *Spectrochim. Acta, A* **204** (2018) 150 (<https://doi.org/10.1016/j.saa.2018.06.046>)

370 11. X. Muñoz, D. Clofent, M. J. Cruz, *Curr. Opin. Allergy Clin. Immunol.* **23** (2023) 70
371 (<https://doi.org/10.1097/aci.0000000000000885>)

372 12. S. Shahabuddin, R. Khanam, M. Khalid, N. M. Sarih, J. J. Ching, S. Mohamad, R. Saidur,
373 *Arabian J. Chem.* **11** (2018) 1000 (<https://doi.org/10.1016/j.arabjc.2018.05.004>)

374 13. S. Rafaqat, N. Ali, C. Torres, B. Rittmann, *RSC Adv.* **12** (2022) 17104
375 (<https://doi.org/10.1039/D2RA01831D>)

376 14. S. Khan, T. Noor, N. Iqbal, L. Yaqoob, *ACS Omega* **9** (2024) 21751
377 (<https://doi.org/10.1021/acsomega.4c00887>)

378 15. S. Dutta, B. Gupta, S. K. Srivastava, A. K. Gupta, *Mater. Adv.* **2** (2021) 4497
379 (<https://doi.org/10.1039/D1MA00354B>)

380 16. S. Goudjil, S. Guergazi, T. Masmoudi, S. Achour, *Desalin. Water Treat.* **209** (2021) 429
381 (<https://doi.org/10.5004/dwt.2021.26474>)

382 17. R. Zhao, S. Zong, Q. Ma, Z. Xu, J. Yuan, *Sci. Rep.* **15** (2025) 6306
383 (<https://doi.org/10.1038/s41598-024-75153-2>)

384 18. T. Cui, X. Wang, Y. Chen, Y. Chen, B. Fu, Y. Tu, *Water Resour. Ind.* **30** (2023) 100217
385 (<https://doi.org/10.1016/j.wri.2023.100217>)

386 19. G. Zeng, X. Liu, L. Wu, Z. Meng, D. Zeng, C. Yu, *Chin. J. Struct. Chem.* **43** (2024)
387 100462 (<https://doi.org/10.1016/j.cjsc.2024.100462>)

388 20. F. J. Benitez, J. L. Acero, F. J. Real, *J. Hazard. Mater.* **89** (2002) 51
389 ([https://doi.org/10.1016/S0304-3894\(01\)00300-4](https://doi.org/10.1016/S0304-3894(01)00300-4))

390 21. K. Rajeshwar, M. Osugi, W. Chanmanee, C. Chenthamarakshan, M. V. B. Zanoni, P.
391 Kajitvichyanukul, R. Krishnan-Ayer, *J. Photochem. Photobiol., C* **9** (2008) 171
392 (<https://doi.org/10.1016/j.jphotochemrev.2008.09.001>)

393 22. V. K. Gupta, R. Saravanan, S. Agarwal, F. Gracia, M. M. Khan, J. Qin, R. V.
394 Mangalaraja, *J. Mol. Liq.* **232** (2017) 423 (<https://doi.org/10.1016/j.molliq.2017.02.095>)

395 23. A. H. Majeed, L. A. Mohammed, O. G. Hammoodi, S. Sehgal, M. A. Alheety, K. K.
396 Saxena, S. A. Dadoosh, I. K. Mohammed, M. M. Jasim, N. U. Salmaan, *Int. J. Polym.
397 Sci.* **2022** (2022) 9047554 (<https://doi.org/10.1155/2022/9047554>)

398 24. J. Luo, S. Jiang, R. Liu, Y. Zhang, X. Liu, *Electrochim. Acta* **96** (2013) 103
399 (<https://doi.org/10.1016/j.electacta.2013.02.072>)

400 25. M. Deyab, G. Mele, E. Bloise, Q. Mohsen, *Sci. Rep.* **11** (2021) 12371
401 (<https://doi.org/10.1038/s41598-021-91688-0>)

402 26. J. Upadhyay, T. M. Das, R. Borah, *Int. J. Polym. Anal. Charact.* **26** (2021) 354
403 (<https://doi.org/10.1080/1023666X.2021.1891799>)

404 27. C. Abdul Kadar, M. Faisal, N. Maruthi, N. Raghavendra, B. Prasanna, S. Manohara,
405 *Macromol. Res.* **30** (2022) 638 (<https://doi.org/10.1007/s13233-022-0067-z>)

406 28. A. Samadi, M. Xie, J. Li, H. Shon, C. Zheng, S. Zhao, *Chem. Eng. J.* **418** (2021) 129425
407 (<https://doi.org/10.1016/j.cej.2021.129425>)

408 29. R. Jamal, L. Zhang, M. Wang, Q. Zhao, T. Abdiryim, *Prog. Nat. Sci.: Mater. Int.* **26**
409 (2016) 32 (<https://doi.org/10.1016/j.pnsc.2016.01.001>)

410 30. G. Gustafsson, Y. Cao, G. M. Treacy, F. Klavetter, N. Colaneri, A. J. Heeger, *Nature* **357**
411 (1992) 477 (<https://doi.org/10.1038/357477a0>)

412 31. T. Anirudhan, S. Rejeena, *J. Mater.* **2015** (2015) 636409
413 (<https://doi.org/10.1155/2015/636409>)

414 32. V. J. Mayani, S. V. Mayani, S. W. Kim, *Sci. Rep.* **7** (2017) 7239
415 (<https://doi.org/10.1038/s41598-017-07707-6>)

416 33. R. Manivannan, J. Ryu, Y.-A. Son, *Colloids Surfaces, A* **608** (2021) 125601
417 (<https://doi.org/10.1016/j.colsurfa.2020.125601>).